

Granular binary mixtures improve energy dissipation efficiency of granular dampers

Nydia Roxana Varela-Rosales · Angel Santarossa · Michael Engel · Thorsten Pöschel

Received: February 8, 2023/ Accepted: date

Abstract Granular dampers are systems used to attenuate undesired vibrations produced by mechanical devices. They consist of cavities filled by granular particles. In this work, we consider a granular damper filled with a binary mixture of frictionless spherical particles of the same material but different size using numerical discrete element method simulations. We show that the damping efficiency is largely influenced by the composition of the binary mixture.

Keywords granular damper, vibration, energy dissipation, granular mixtures

1 Introduction

Granular dampers are devices that exploit the dissipative nature of granular interactions to passively attenuate vibrations. In their most simple design, they consist of an enclosure partially filled by granular particles. When subjected to mechanical vibrations, the particles collide with each other and with the walls of the enclosure, thus, inelastic interactions (particle-particle and particle-wall) dissipate mechanical energy into heat. Granular dampers reveal distinctive characteristics beneficial for their application in technical devices: The design of granular dampers is simple and requires a minimum of maintenance, which makes them interesting for aerospace technologies [1] and applications in weightlessness [2–4]. They operate across a wide

range of temperature [5], making them particularly useful in harsh environments. Due to these features, granular dampers have numerous technical applications for instance in medicine [6], construction [7], and in the vibration control during earthquakes [8–10].

Granular dampers are subject to research for a long time, also using numerical discrete element method (DEM) simulation techniques [11–13]. In numerical studies and in experiments, it has been shown that the performance of granular dampers is sensitive to a variety of parameters such as the mass ratio between the granulate and the container [14], number and material of the particles [15, 16], particle size [17, 18, 1] and shape [19], size and shape of the enclosure [20–22], the free volume inside the container (gap clearance) [23, 24], and others [25–27]. Yet, the effect of particle size dispersion on the efficiency of granular dampers was much less investigated. Only recently, the addition of micrometer-sized particles to a system of millimeter-sized monodisperse spheres was reported to have a significant effect on damping performance [21]. An explanation of this effect, as well as the influence of the dispersion on damping efficiency in general remain open questions.

In this paper, we consider granular dampers using bidisperse granular mixtures by means of DEM simulation, which is reliable numerical tool to study granular systems [28, 29].

2 System setup and numerical model

Our damper of cubical shape ($8 \times 8 \times 8 \text{ cm}^3$) is filled partially by N frictionless spheres. For both container and particles, we assume the same material characteristics corresponding to steel (density $\rho = 7,850 \text{ kg/m}^3$, Young modulus $E = 2 \times 10^9 \text{ Pa}$, Poisson ratio $\nu = 0.3$).

Nydia Roxana Varela-Rosales · Angel Santarossa · Michael Engel · Thorsten Pöschel
Institute for Multiscale Simulations
Friedrich-Alexander-Universität Erlangen-Nürnberg
Cauerstraße 3, 91058 Erlangen
Germany
E-mail: thorsten.poeschel@fau.de

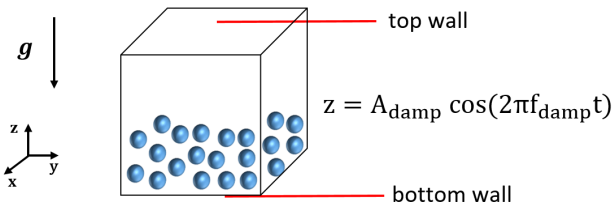


Fig. 1: Sketch of the granular damper. The walls of the enclosure in z direction are referred to as top and bottom walls, respectively.

The damper is driven by oscillations, $z(t) = A_{\text{damp}} \cos(2\pi ft)$ with $f_{\text{damp}} = 70$ Hz where gravity, $g = 9.8 \text{ m/s}^2$, acts in negative z direction. Figure 1 shows a sketch of the setup.

The interaction force between viscoelastic frictionless spheres is given by the elastic Hertz law [30] and an appropriate dissipative force. The Hertz law results from the assumption that the elastic stress is a linear function of the strain, therefore, for the dissipative force it is reasonable to assume that the dissipative stress is a linear function of the strain rate [31]. Combining these forces, we obtain the absolute value of the force between particles i and j of radii R_i and R_j at positions \vec{r}_i and \vec{r}_j at velocities \vec{v}_i and \vec{v}_j . When in contact, that is, if $\xi_{ij} \equiv R_i + R_j - |\vec{r}_i - \vec{r}_j| \geq 0$, the force is

$$F_{ij} = \frac{2E\sqrt{R_{ij}^{\text{eff}}}}{3(1-\nu^2)} \left(\xi^{3/2} + A\sqrt{\xi}\dot{\xi} \right) \quad (1)$$

$$\vec{F}_{ij} = \max(0, F_{ij}) \frac{\vec{r}_i - \vec{r}_j}{|\vec{r}_i - \vec{r}_j|}, \quad (2)$$

with $1/R_{ij}^{\text{eff}} \equiv 1/R_i + 1/R_j$. The dissipative constant, A , is a function of the viscosities of the particles' materials [31], which are difficult to determine. A much easier way to determine A is through the coefficient of restitution at a certain impact rate [32]. For our simulations, to determine A , we assume the coefficient of restitution $\varepsilon = 0.75$ for steel particles colliding at impact rate 1 m/s. For bidisperse mixtures, we obtain A for the collision of particles of each species and calculate its arithmetic mean. In some cases, it can happen that the dissipative force overcompensates the restoring elastic force, resulting in a total attractive force (see [28] for a detailed explanation). The maximum rule in Eq. 2 ensures that the interaction force is always repulsive. In our force model, we neglect frictional forces between contacting particles, justified by previous evidence [33, 34, 19], which shows that the main dissipation mechanism in granular dampers is due to normal interaction forces. For our DEM simulations, we use Yade [35].

3 Energy dissipation per cycle of oscillation

We quantify energy dissipation efficiency by

$$E_d(t) \equiv \frac{(E_{\text{pp}} + E_{\text{pw}})}{E_{\text{max}}}, \quad (3)$$

where E_{pp} is given by

$$E_{\text{pp}}(t) = \frac{1}{2T} \int_t^{t+T} \sum_{i=1}^N \sum_{i \neq j}^N \vec{F}_{ij} \cdot (\vec{v}_j - \vec{v}_i) dt, \quad (4)$$

and E_{pw} by

$$E_{\text{pw}}(t) = \frac{1}{T} \int_t^{t+T} \sum_{i=1}^N \sum_{w=1}^M \vec{F}_i^w \cdot \vec{v}_i dt, \quad (5)$$

with $T = 1/f$. Equation (3) relates the energy dissipated by particle-particle (E_{pp}) and particle-wall (E_{pw}) contacts during one period T of oscillation to the maximum energy, E_{max} , that can be dissipated in one oscillation cycle. The quantity E_{max} was defined in [2]. It is obtained by assuming that all particles collide twice per cycle with the bottom and top walls of the container at maximal relative velocity and dissipate the energy of the relative motion in each of these collisions.

Note that E_d is similar but not identical to the quantity b defined in Eq. (4) of [13], which relates the dissipated energy to the total kinetic energy.

The dissipated energy depends on the dynamics of the granulate and is, thus, a fluctuating quantity. Therefore, we compute an average, $\langle E_d \rangle$, from a linear fit to $E_d(t)$.

4 Modes of operation of granular dampers

When operating in weightlessness, depending on the amplitude, A_{damp} , of the oscillation, granular dampers reveal different modes [2]. For small A_{damp} , the granular material exhibits gas-like behavior. In this state, only a small fraction of the kinetic energy is dissipated. More relevant for granular damping is the *collect-and-collide* regime [34] observed for large A_{damp} , where the center of mass of the granulate moves synchronously with the container. In this state, during the inward stroke, the granulate accumulates at the wall of the container forming a packed layer. When the acceleration of the box decreases, this layer leaves the wall collectively and eventually collides with the opposing wall where a large fraction of the kinetic energy is dissipated. The modes of operation are separated by a sharp transition at a critical value of A_{damp} ; here the dissipated energy per oscillation achieves its maximum value [2, 4]. Motivated

by this argument, in the results section, we consider the interval $A_{\text{damp}} \in [2, 4]$ cm containing the critical value.

A more detailed classification of modes of behavior of vibrated boxes filled by granular material was presented in [36], however, not in the context of granular damping.

5 Results

5.1 Classes of equal binary mixtures

We consider three classes of binary mixtures in comparison with a monodisperse reference system: (a) the total mass of the granulate (M_{tot}) in the bidisperse system equals the mass in the monodisperse reference system, but not the number of particles; (b) the total number of particles (N_{tot}) in the bidisperse system equals the number of particles in the reference system, but not the total mass of the granulate; (c) both the number of particles and the mass of the granulate in the bidisperse system equal the corresponding quantities in the monodisperse reference system, thus, isolating the effect of size dispersion from particle number and mass. We summarize the properties of the classes (a)-(c) in Tab. 1.

	large particles	small particles	quantities conserved
reference system	$N_{\text{ref}} = 300$, $R_{\text{ref}} = 0.25$ cm, $M_{\text{ref}} = 0.154$ kg		
class (a) $\sigma \in [0.1, 0.9]$	$N_{\text{tot}}/2$ $R = R_{\text{ref}}$	$N_{\text{tot}}/2$ $R = \sigma R_{\text{ref}}$	$M_{\text{tot}} = M_{\text{ref}}$
class (b) $\sigma \in [0.1, 0.9]$	$N_{\text{ref}}/2$ $R = R_{\text{ref}}$	$N_{\text{ref}}/2$ $R = \sigma R_{\text{ref}}$	$N_{\text{tot}} = N_{\text{ref}}$
class (c) $\sigma \in [0.1, 0.9]$ $\hat{\sigma}^3 = 2 - \sigma^3$	$N_{\text{ref}}/2$ $R = \hat{\sigma} R_{\text{ref}}$	$N_{\text{ref}}/2$ $R = \sigma R_{\text{ref}}$	$N_{\text{tot}} = N_{\text{ref}}$ $M_{\text{tot}} = M_{\text{ref}}$

Table 1: Classes of binary mixtures studied in this work.

5.2 Class (a): Equal total mass

Figure 2 shows the average energy dissipation efficiency per cycle, $\langle E_d \rangle$, normalized by the total mass, m , of the granulate, as a function of the vibration amplitude for different size ratios, σ . For all values of σ , the system reveals a similar behavior. An optimal value of the driving amplitude, A_{opt} , divides the dynamics into two regimes: For $A_{\text{damp}} \lesssim 2.8$ cm, the granulate is in a gaseous state where only a small fraction of the particles collides with the walls during an oscillation period. In contrast, for $A_{\text{damp}} \gtrsim 2.8$ cm, the center of mass of the granulate

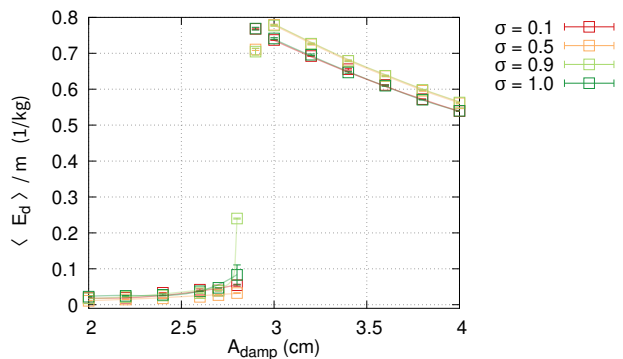


Fig. 2: Class (a): Energy dissipation per cycle of oscillation, $\langle E_d \rangle$, normalized by the mass, m , of the granulate, as a function of the driving amplitude. For each value of σ , the data was averaged over 50 periods. Error bars show the standard deviation.

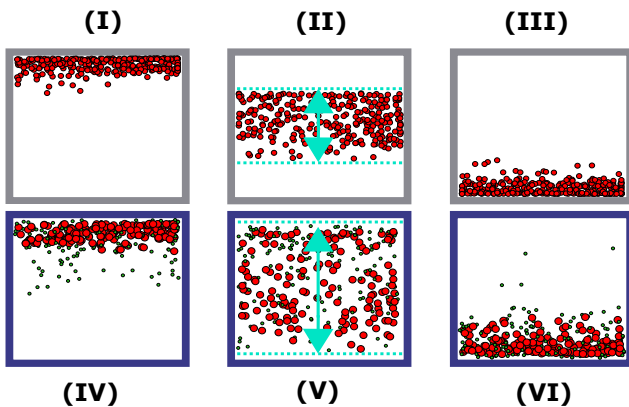


Fig. 3: Class (a): Snapshots of the monodisperse reference system (grey boxes) at the times of minimal (I),(III) and maximal (II) velocity and the same for a bidisperse granulate blue boxes with $\sigma = 0.1$ (IV)-(VI). Dotted lines in (II), (V) indicate the region populated by particles. Red circles show particles with radius $R = R_{\text{ref}}$, green circles show small particles, $R = \sigma R_{\text{ref}}$.

moves synchronously with the external driving, in the collect-and-collide regime. Both modes of dynamic behavior, gaseous and collect-and-collide, and their dissipative properties are discussed in detail in [2–4, 34].

Figure 3 shows snapshots of the simulation at the times of minimal and maximal velocity for the reference system and for a bidisperse system with $\sigma = 0.1$ in the collect-and-collide regime. We notice that for bidisperse systems the particles spread over a larger volume in the container. Moreover, we observe size segregation.

For $A_{\text{damp}} > A_{\text{opt}}$ (Fig. 2), the bidisperse system with $\sigma = 0.5$ achieves higher values of $\langle E_d \rangle / m$ than the reference system, i.e., it dissipates energy more effi-

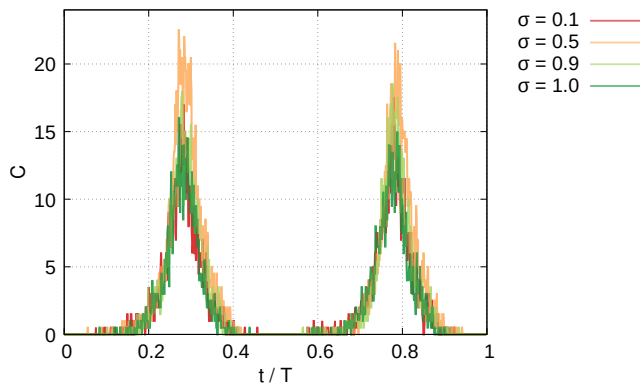


Fig. 4: Class (a): Number of particles C in contact with the bottom or top wall as a function of time, for $A_{\text{damp}} = 3$ cm. For each value of σ , the data was averaged over 50 periods.

ciently than the monodisperse reference system, in the collect-and-collide mode.

To understand this behaviour, we consider the particles' collisions with the top and bottom walls, which dominate the dissipation [33]. In each time step of the integration, we record the number of particles contacting one of these walls (Fig. 4). We note that for bidisperse systems, the collision frequency is higher than for the reference system ($\sigma = 1$). Detailed analysis shows that this difference can be attributed to collisions of small particles with the walls.

The number of particle contacts alone is, however, not sufficient to explain the difference in energy dissipation. Therefore, we record the force in z direction (F_z) exerted by the granulate on the top and bottom walls (Fig. 5). The bidisperse damper with $\sigma = 0.5$ show a higher value of F_z , compared to the reference system. Higher absolute values of F_z lead to higher momentum transfer and, in turn, to larger loss of kinetic energy in dissipative collisions, which explains the difference in the energy dissipation efficiency shown in Fig. 2.

5.3 Class (b): Equal number of particles

Figure 6 shows the average energy dissipation efficiency per cycle, $\langle E_d \rangle$, normalized by the total mass, m , of the granulate, as a function of the vibration amplitude for different size ratios, σ , corresponding to Fig. 2 for class (a) binary mixtures. For all values of σ , the systems exhibit a similar behavior. Again, we see two regimes for small and large amplitude (gaseous and collect-and-collide) and again dissipation efficiency for bidisperse mixtures exceeds that of the reference system ($\sigma = 1$).

From Fig. 7 we observe that the number of contacts

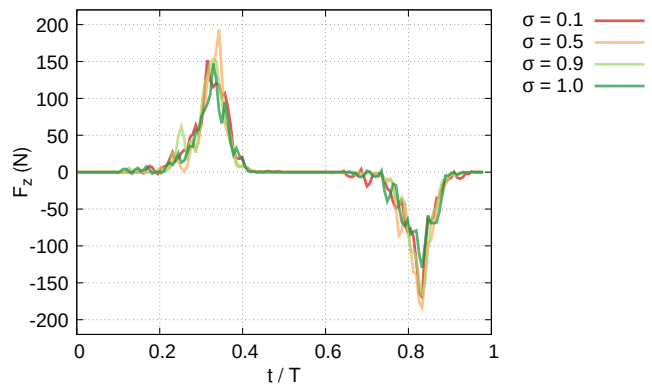


Fig. 5: Class (a): Force in z direction exerted on the bottom and top wall as a function of time, for $A_{\text{damp}} = 3$ cm. For each value of σ , the data was averaged over 50 periods.

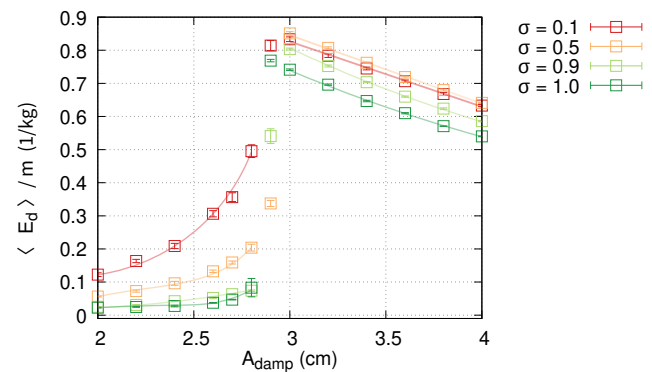


Fig. 6: Class (b): Energy dissipation per cycle of oscillation, $\langle E_d \rangle$, normalized by the mass, m , of the granulate, as a function of the driving amplitude. For each value of σ , the data was averaged over 50 periods. Error bars show the standard deviation.

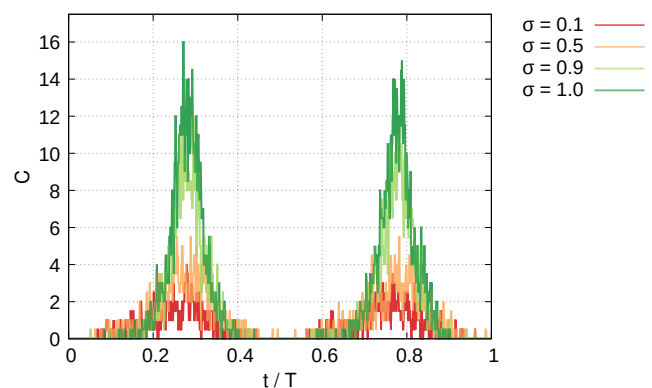


Fig. 7: Class (b): Number of particles C in contact with the bottom or top wall as a function of time, for $A_{\text{damp}} = 3$ cm. For each value of σ , the data was averaged over 50 periods.

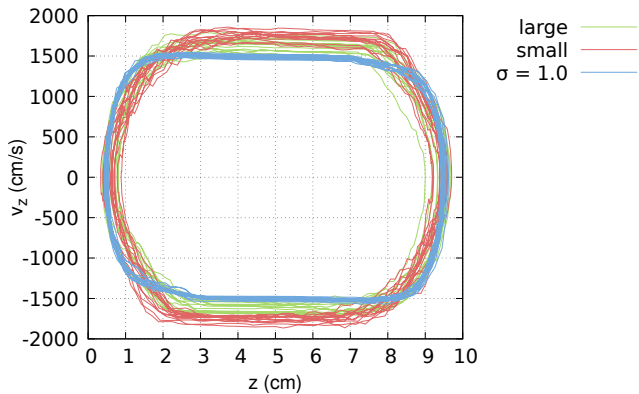


Fig. 8: Class (b): Phase plot, $v_z(z)$, of the z -component of the center-of-mass position for $\sigma = 1$ (reference) and $\sigma = 0.5$. Amplitude is $A_{\text{damp}} = 3$ cm. For the bidisperse system, the plot is performed separately for small and large particles.

with the top and bottom walls of the reference system ($\sigma = 1$) exceeds that of mixtures for all values $\sigma < 1$. Consequently, the difference of the dissipation shown in Fig. 6 cannot be attributed to the number of contacts.

From the phase plot of the center-of-mass position in the direction of the oscillation, z , (Fig. 8), we see that both small and large particles of the bidisperse system (with $\sigma = 0.5$) assume larger velocities than the particles of the reference system ($\sigma = 1$). Higher absolute velocities give rise to higher impact velocities and, thus, larger loss of kinetic energy in dissipative collisions, which explains the difference in the damping efficiency shown in Fig. 6.

5.4 Class (c): Equal total mass and number of particles

Similar as for the previous classes, also for class (c) $\langle E_d \rangle / m$, as a function of A_{damp} (Fig. 9), shows two well separated regimes for large and small A_{damp} . In contrast to classes (a) and (b), here the transition value of A_{damp} depends on σ . Also in contrast to classes (a) and (b), here the values of $\langle E_d \rangle / m$ of monodisperse reference system for $A_{\text{damp}} > 2.8$ cm exceed the values of dampers with $\sigma < 1$. Here, the number of contacts (Fig. 10) of the reference system exceeds the value for the granular mixtures. Furthermore, the force in z direction, F_z , (Fig. 11), exerted by the particles of the reference system is considerably larger than for bidisperse dampers.

From the phase plot for $\sigma = 0.5$, Fig. 12, we see that the large particles follow approximately the same path as the particles of the reference system while the small particles achieve larger velocities. Large and small par-

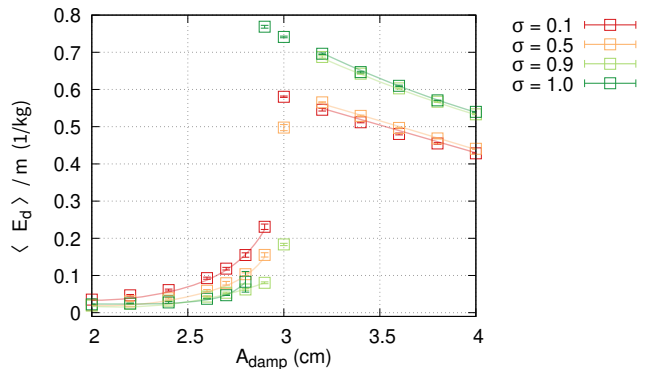


Fig. 9: Class (c): Energy dissipation per cycle of oscillation, $\langle E_d \rangle$, normalized by the mass, m , of the granulate, as a function of the driving amplitude. For each value of σ , the data was averaged over 50 periods. Error bars show the standard deviation. In contrast to classes (a) and (b), here we find more efficient dissipation for the reference system ($\sigma = 1$) than for bidisperse systems.

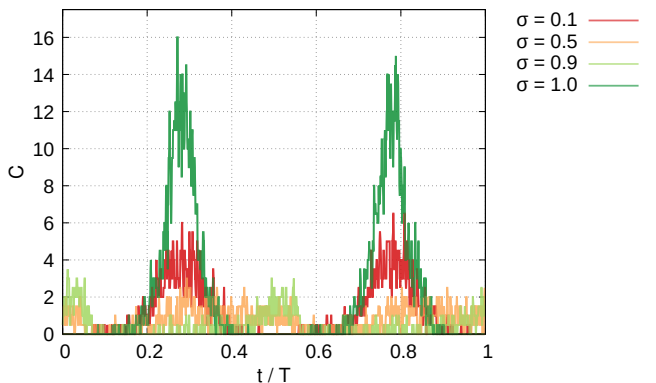


Fig. 10: Class (c): Number of particles C in contact with the bottom or top wall as a function of time, for $A_{\text{damp}} = 3$ cm. For each value of σ , the data was averaged over 50 periods.

ticles in the bidisperse system do not move collectively. In contrast to dampers of class (b), there is no energy dissipation enhancement due to a higher center of mass velocity of both large and small particles.

6 Conclusion

The efficiency of granular dampers operating with a bidisperse granular mixture depends sensitively on the composition of the mixture. Thus, the choice of the composition can enhance energy dissipation in granular dampers significantly as compared to granular dampers operating with a monodisperse granulate of the same material. For the comparison with a monodisperse ref-

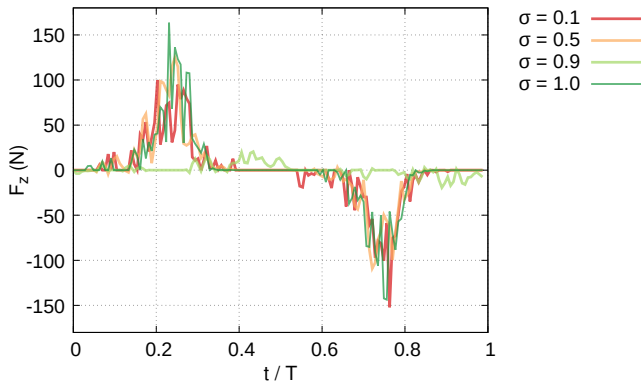


Fig. 11: Class (c): Force in z direction exerted on the bottom and top wall as a function of time, for $A_{\text{damp}} = 3$ cm. For each value of σ , the data was averaged over 50 periods.

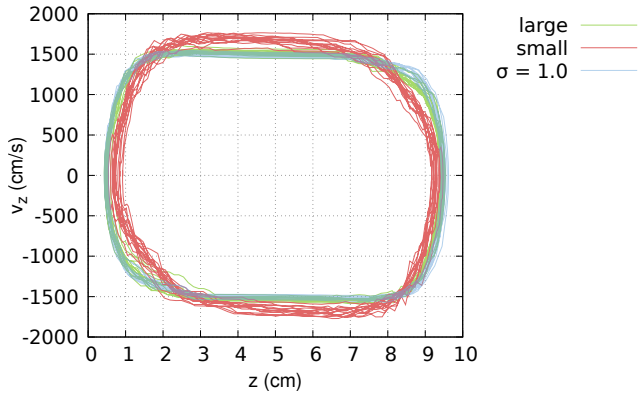


Fig. 12: Class (c): Phase plot, $v_z(z)$, of the z -component of the center-of-mass position for $\sigma = 1$ (reference) and $\sigma = 0.5$. Amplitude is $A_{\text{damp}} = 3$ cm. For the bidisperse system, the plot is performed separately for small and large particles.

reference system, we considered three classes of mixtures: (a) both monodisperse and bidisperse systems are of the same total mass of the granulate (but different number of particles); (b) both systems have the same total number of particles (but different mass); (c) the sizes of the particles in the mixture are scaled such that both systems contain the same number of particles of the same total mass.

For dampers of class (a), the efficiency increases due to a larger frequency of collisions and higher exerted force during impact with the top and bottom walls in comparison with the reference system.

For dampers of class (b), the efficiency increases due to the larger relative velocity between the granular particles and the wall of the container, shown by the phase

plot of the center of mass velocity of the binary system in comparison with the monodisperse reference system.

For dampers of class (c), the energy dissipation efficiency is smaller than for the monodisperse reference system due to a smaller frequency of collisions and lower exerted force during impact with the top and bottom walls. Furthermore, there is no energy dissipation improvement due to a higher center of mass velocity of both large and small particles.

In conclusion, we find that the dissipative properties of mixtures of differently sized particles differ from the dissipative properties of monodisperse systems. Therefore, the particle size distribution of the granulate is an important feature for the design of granular dampers.

Acknowledgements The work was supported by the Interdisciplinary Center for Nanostructured Films (IZNF), the Competence Unit for Scientific Computing (CSC), and the Interdisciplinary Center for Functional Particle Systems (FPS) at Friedrich-Alexander University Erlangen-Nürnberg. N. R. V.-R. and M. E. acknowledge funding by the Deutsche Forschungsgemeinschaft (DFG) through project number 406658237. A. S. and T. P. acknowledge funding by DFG under project number 411517575 and through the Research Training Group GRK 2423 “Fracture across Scales –FRASCAL”.

Compliance with ethical standards

The authors declare that they have no conflict of interest.

References

1. H. V. Panossian. Structural damping enhancement via non-obstructive particle damping technique. *J. Vib. Acoust.*, 114:101–105, 1992. doi: 10.1115/1.2930221.
2. A. Sack, M. Heckel, J. E. Kollmer, F. Zimmer, and T. Pöschel. Energy dissipation in driven granular matter in the absence of gravity. *Phys. Rev. Lett.*, 111:018001, 2013. doi: 10.1103/PhysRevLett.111.018001.
3. A. Sack, M. Heckel, J. E. Kollmer, and T. Pöschel. Probing the validity of an effective-one-particle description of granular dampers in microgravity. *Granul. Matter*, 17:73–82, 2015. doi: 10.1007/s10035-014-0539-8.
4. A. Sack, K. Windows-Yule, M. Heckel, D. Werner, and T. Pöschel. Granular dampers in microgravity: sharp transition between modes of operation. *Granul. Matter*, 22:54, 2020. doi: 10.1007/s10035-020-01017-x.
5. Z. Xia, X. Liu, Y. Shan, and X. Li. Coupling simulation algorithm of discrete element method and

- finite element method for particle damper. *J. Low Freq. Noise Vib. Act. Control*, 28:197–204, 2009. doi: 10.1260/026309209790252545.
6. M. Heckel, A. Sack, J. E. Kollmer, and T. Pöschel. Granular dampers for the reduction of vibrations of an oscillatory saw. *Physica*, A391:4442–4447, 2012. doi: 10.1016/j.physa.2012.04.007.
 7. Z. Xu, M. Y. Wang, and T. Chen. An experimental study of particle damping for beams and plates. *J. Vib. Acoust.*, 126:141–148, 2004. doi: 10.1115/1.1640354.
 8. F. Naeim, M. Lew, L. D. Carpenter, N. F. Youssef, F. Rojas, G. R. Saragoni, and M. S. Adaros. Performance of tall buildings in Santiago, Chile during the 27 February 2010 offshore Maule, Chile earthquake. *Struct. Design Tall Spec. Build.*, 20:1–16, 2011. doi: 10.1002/tal.675.
 9. Z. Lu, X. Lu, W. Lu, and S. F. Masri. Experimental studies of the effects of buffered particle dampers attached to a multi-degree-of-freedom system under dynamic loads. *J. Sound Vib.*, 331:2007–2022, 2012. doi: 10.1016/j.jsv.2011.12.022.
 10. Y. Zhou, D. Li, F. Shi, W. Luo, and X. Deng. Experimental study on mechanical properties of the hybrid lead viscoelastic damper. *Eng. Struct.*, 246:113073, 2021. doi: 10.1016/j.engstruct.2021.113073.
 11. C. Salueña, S. E. Esipov, T. Pöschel, and S. S. Simonian. Dissipative properties of granular ensembles. *SPIE: Smart Structures and Materials 1998: Passive Damping and Isolation*, 3327:23–31, 1998. doi: 10.1117/12.310696.
 12. C. Salueña, S. E. Esipov, D. Rosenkranz, and H. V. Panossian. Modeling of arrays of passive granular dampers. *SPIE: Smart Structures and Materials: Passive Damping and Isolation*, 3672:32, 1999. doi: 10.1117/12.349800.
 13. C. Salueña, T. Pöschel, and S. E. Esipov. Dissipative properties of vibrated granular materials. *Phys. Rev. E*, 59:4422–4425, 1999. doi: 10.1103/PhysRevE.59.4422.
 14. X. Wang, X. Liu, Y. Shan, and T. He. Design, simulation and experiment of particle dampers attached to a precision instrument in spacecraft. *J. Vibroengineering*, 17:1605–1614, 2015. doi: 10.1177/16878140211044923.
 15. K. Hashemnia. Effect of particle size and media volume fraction on the vibration attenuation of a thin-walled beam containing granular media. *Soil Dyn. Earthq. Eng.*, 147:106816, 2021. doi: 10.1016/j.soildyn.2021.106816.
 16. Daniel N. J. Els. Damping of rotating beams with particle dampers: experimental analysis. *AIAA J.*, 49:2228–2238, 2011. doi: 10.2514/1.J050984.
 17. A. Papalou and S. F. Masri. An experimental investigation of particle dampers under harmonic excitation. *J. Vib. Control*, 4:361–379, 1998. doi: 10.1177/107754639800400402.
 18. T. Chen, K. Mao, X. Huang, and M. Y. Wang. Dissipation mechanisms of nonobstructive particle damping using discrete element method. *SPIE: Smart Structures and Materials: Passive Damping and Isolation*, 4331:294, 2001. doi: 10.1117/12.432713.
 19. H. Pourtavakoli, E. J. R. Parteli, and T. Pöschel. Granular dampers: does particle shape matter? *New J. Phys.*, 18:073049, 2016. doi: 10.1088/1367-2630/18/7/073049.
 20. J. E. Kollmer, A. Sack, M. Heckel, and T. Pöschel. Relaxation of a spring with an attached granular damper. *New J. Phys.*, 15, 2013. doi: 10.1088/1367-2630/15/9/093023.
 21. N. Meyer and R. Seifried. Toward a design methodology for particle dampers by analyzing their energy dissipation. *Comput. Part. Mech.*, 8:681–699, 2021. doi: 10.1007/s40571-020-00363-0.
 22. M. V. Ferreyra, J. M. Gó-Paccapelo, R. Suarez, and L. A. Pugnaloni. Avoiding chaos in granular dampers. *EPJ Web of Conferences*, 249:15003, 2021. doi: 10.1051/epjconf/202124915003.
 23. Y. Wang, B. Liu, A. Tian, and W. Tang. Experimental and numerical investigations on the performance of particle dampers attached to a primary structure undergoing free vibration in the horizontal and vertical directions. *J. Sound Vib.*, 371:35–55, 2016. doi: 10.1016/j.jsv.2016.01.056.
 24. K. Zhang, T. Chen, X. Wang, and J. Fang. Rheology behavior and optimal damping effect of granular particles in a non-obstructive particle damper. *J. Sound Vib.*, 364:30–43, 2016. doi: 10.1016/j.jsv.2015.11.006.
 25. M. V. Ferreyra, M. Baldini, L. A. Pugnaloni, and S. Job. Effect of lateral confinement on the apparent mass of granular dampers. *Granul. Matter*, 23:45, 2021. doi: 10.1007/s10035-021-01090-w.
 26. Z. Lu, X. Lu, H. Jiang, and S. F. Masri. Discrete element method simulation and experimental validation of particle damper system. *Engineering Computations*, 31:810–823., 2014. doi: 10.1108/EC-08-2012-0191.
 27. M. Sánchez, G. Rosenthal, and L. A. Pugnaloni. Universal response of optimal granular damping devices. *J. Sound Vib.*, 331:4389–4394, 2012. doi: 10.1016/j.jsv.2012.05.001.
 28. T. Pöschel and T. Schwager. *Computational Granular Dynamics: Models and Algorithms*. Springer,

2005. doi: 10.1007/3-540-27720-X.
29. H.-G. Matuttis and J. Chen. *Understanding the Discrete Element Method: Simulation of Non-Spherical Particles for Granular and Multi-Body Systems*. Wiley, 2014. doi: 10.1002/9781118567210.
 30. H. Hertz. Ueber die Berührung fester elastischer Körper. *J. reine und angewandte Math.*, 92:156–171, 1881. doi: 10.1515/crll.1882.92.156.
 31. N. V. Brilliantov, F. Spahn, J.-M. Hertzsch, and T. Pöschel. Model for collisions in granular gases. *Phys. Rev. E*, 53:5382–5392, 1996. doi: 10.1103/PhysRevE.53.5382.
 32. P. Müller and T. Pöschel. Collision of viscoelastic spheres: Compact expressions for the coefficient of normal restitution. *Phys. Rev. E*, 84:021302, 2011. doi: 10.1103/PhysRevE.84.021302.
 33. X.-M. Bai, L. M. Keer, Q. J. Wang, and R. Q. Snurr. Investigation of particle damping mechanism via particle dynamics simulations. *Granul. Matter*, 11:417, 2009. doi: 10.1007/s10035-009-0150-6.
 34. M. N. Bannerman, J. E. Kollmer, A. Sack, M. Heckel, P. Mueller, and T. Pöschel. Movers and shakers: Granular damping in microgravity. *Phys. Rev. E*, 84:011301, 2011. doi: 10.1103/PhysRevE.84.011301.
 35. V. Šmilauer, V. Angelidakis, E. Catalano, R. Caulk, B. Chareyre, W. Chèvremont, S. Dorofeenko, J. Duriez, N. Dyck, Eliáš, B. Er, A. Eulitz, A. Gladky, N. Guo, C. Jakob, F. Kneib, J. Kozicki, D. Marzougui, R. Maurin, C. Modenese, G. Pekmezi, L. Scholtès, L. Sibille, J. Stránský, T. Sweijen, K. Thoeni, and C. Yuan. *Yade Documentation*. 2021. doi: 10.5281/zenodo.5705394.
 36. E. Opsomer, F. Ludewig, and N. Vandewalle. Phase transitions in vibrated granular systems in microgravity. *Phys. Rev. E*, 84:051306, 2011. doi: 10.1103/PhysRevE.84.051306.